

Origin of light nuclei in near earth orbit

L.Derome and M. Buénerd

Institut des Sciences Nucléaires, IN2P3, 53 av. des Martyrs, 38026 Grenoble cedex, France

abstract: The possible sources of light nuclei populations observed recently below the geomagnetic cutoff by the AMS experiment are discussed in terms of nuclear processes: fragmentation of the incoming flux of cosmic ^4He on atmospheric nuclei, and nuclear coalescence from proton and ^4He induced reactions. Results of simulations for $^2,3\text{H}$ and $^3,4\text{He}$, are presented and compared to the data.

The study of particle populations in the earth environment has a long and rich history covering the last few decades (see [1] for a general overview of the subject, and the references in [2, 3] for details). After a period of waning activity, the topic is likely to regain interest with the occurrence of a new generation of balloon and satellite experiments, which open prospects for data samples of unmatched quantity and quality. This is well illustrated with the new data obtained recently in orbit close to earth by the precursor flight of the AMS experiment, which achieved on its orbit, a set of high accuracy measurements of charged particle flux over a wide range of latitude. New features of the proton [2, 4] and lepton [3] flux have been uncovered, and surprisingly large values of flux measured below the geomagnetic cutoff (GC). These features have been successfully interpreted in previous works by the authors [5, 6], referred to as I in the following. In addition, small but significant populations of ^3He and deuterium (D or ^2H) particles were also measured below GC, with kinetic energies extending beyond 1 GeV per nucleon [7, 8]. This paper completes a set of three reports devoted to the interpretation of the new AMS data. Its purpose is to investigate the possible origins of the measured ^3He and D flux using the same approach as reported in I.

Since particles below GC cannot be primary cosmic rays (CR), they have to be produced by nuclear reactions between incoming CRs (mainly p and ^4He), and atmospheric nuclei (mainly ^{14}N and ^{16}O). The pattern of $Z=2$ particle spectra observed above and below GC is highly peculiar since only ^4He are observed above GC whereas only ^3He are found below GC, with however a small admixture of the other isotope being compatible with the data in both cases [7]. This pattern, together with the relative population of light nuclei, provide clues to the dynamical origin of the subGC particles (or Albedo particles in the geophysical terminology). It can be understood qualitatively and evaluated quantitatively, in terms of the nuclear reaction mechanisms involved in the production process.

Collisions between nuclear systems such as those of interest here, for incident energies beyond the nuclear Fermi energy (≈ 35 MeV/nucleon) region, have very characteristic distributions. The rapidity distributions of reaction products at forward angles display two peaks centered around projectile and target rapidities, corresponding to projectile and target fragmentation in peripheral collisions respectively, and an intermediate plateau between these limits stemming from more central collisions (see for example [9]). Experimentally, the (projectile) fragmentation regime sets in as low as 20 MeV kinetic energy per nucleon [10]. The features of the measured differential cross sections at small angles can be accounted for in the fragmentation model [11], with the width of the fragmentation peak being governed by nuclear motion and nucleon arrangement probability.

With the increasing production angles, the target-like and projectile-like peaks move to the mid-rapidity region, leaving a single broad mid-rapidity peak surviving at the largest angles [9]. This latter kinematical domain is associated to smaller impact parameters and larger energy dissipation due to larger density overlaps in the collisions. In this region, the simple fragmentation picture [11] fails and the description of the collision in terms of the various models based on thermodynamics and spectator-participant pictures [12, 13, 14] are more appropriate. The energy distributions of very light fragments

like 1,2,3H , 3,4He , produced at large scattering angles in such collisions, can be described by means of a variety of models which are all variations approximating more or less successfully the complex multiple nucleon-nucleon scattering processes and nuclear collective effects governing these collisions [12, 15, 16] (see also [13, 14, 17]). In this context, the coalescence model [18, 19] stands as the most successful phenomenological approach of the production cross section for light nuclei, with a remarkable ability to reproducing data over a very wide range of incident energies [14, 17, 20, 21]. In this approach, nucleons coalesce into clusters whenever they fall within the coalescence radius(momentum) in the final state of the collision. Note that the models used here are considered from a purely practical point of view, and not be discussed in their foundations.

For the present purpose, the phenomenological perspective can be summarized the following way: Small production angles are dominated by velocity-conserving projectile-like fragmentation products, while at large angles the coalescence production of light fragments of much lower energy per nucleon, dominates the cross section. In the fragmentation picture, the cross-section is expected to decrease with the decreasing mass number of the (projectile -like) fragment (larger probability for smaller number of nucleon transferred [10, 22]), whereas conversely, in the coalescence model it is decreasing with the increasing fragment mass number (larger probability for smaller cluster mass). In the case of 4He projectile, projectile-like particles are also light fragments, then likely to be produced either by fragmentation or by coalescence, whereas obviously, protons can only induce production of coalescence fragments.

Projectile fragmentation in heavy ion collisions has been extensively studied experimentally in the past [23]. A few 4He fragmentation studies have been reported in the literature over the momentum range of interest here [24, 25, 26]. The production of non velocity-conserving light fragments in p and 4He induced collisions is also fairly well documented experimentally [13, 17, 14].

The 3He spectrum observed in the AMS experiment [7] between the low energy cutoff of the spectrometer and up to about 1 GeV/nucleon (see figures 2 and 3 below), could originate from the two types of reactions described above:

- 1) It could be produced by CR 4He particle fragmentation or fragmentation-like process on atmospheric nuclei (this assumption was also quoted recently in [27]). The quasi absence of subGC 4He is easy to understand in this framework since secondary 4He from fragmentation could only originate from the very small CR flux of heavier nuclei, i.e., mostly ${}^{12}C$ and ${}^{16}O$ (the possible 4He yield from nuclear evaporation being expected at energies below the AMS sensitivity range). However, the basic velocity-conserving property discussed above, is clearly not met here since incident CR 4He have momenta larger than about 6 GeV per nucleon in the equatorial region, while detected 3He and D particles have less than 1 GeV per nucleon (see details below).
- 2) The observed 3He population could also be produced by nuclear coalescence [18] (see [14] for a review of models) from p and 4He induced collisions on atmospheric nuclei [17, 28, 29]. It would explain as well the absence of subGC 4He as discussed above, with a larger population expected below GC for 3He than for 4He particles, by typically one order of magnitude [17], which is compatible with the experimental observation.

The experimental situation then favors the coalescence assumption. The measured flux however, depend on the particular dynamics of each production reaction and of the acceptance of the magnetosphere to the particle considered, and only a detailed investigation can provide a definite answer.

The inclusive spectrum of light nuclei flux at the altitude of AMS (390-400km) have been calculated by means of an evolved version of the same simulation program as described in I. CR protons and Helium 4 are generated with their natural abundance and momentum distributions. They are propagated inside the earth magnetic field using 4th order adaptative Runge-Kutta integration of the equation of motion. They are allowed to interact with atmospheric nuclei and to produce secondary nucleons p, n , 2,3H , and 3,4He , particles with cross sections and multiplicities as discussed below. Each

secondary particle is then propagated and allowed to interact as in the previous step. Only destructive interaction is taken into account for light nuclei, except ${}^4\text{He}$. A reaction cascade can thus develop through the atmosphere. The reaction products are counted when they cross the virtual sphere at the altitude of the AMS spectrometer, upward and downward. All charged particles undergo energy loss by ionisation. Each event is propagated until the particle disappears by nuclear collision, stopping in the atmosphere by energy loss, or escaping to outer space. See I for details. The small production cross section, and then multiplicity, combined with the small magnetosphere acceptance, for the particles of interest here, require a tremendous number of events to be generated, and then a huge computer time, for significant statistics to be reached. This difficulty has been turned around by enhancing numerically the production multiplicity, with the produced events being weighted by the inverse enhancement factor. It has been checked carefully that no distortion of the physics involved could be induced by using this method, in the studied case.

The CR proton and helium flux used in the calculations were those measured by AMS [2, 4, 7]. The values of the total p and ${}^4\text{He}$ reaction cross sections used were based on the parametrization of [30], the latter being checked on the measurements performed on carbon target [31]. The production cross sections for light nuclei have been implemented and run simultaneously in the event generator on the basis of the two models described above.

A) - For the ${}^4\text{He}$ fragmentation cross section, the model from [11] was used. In this model, the fragment production cross section is proportional to $e^{-\frac{P^2}{\sigma^2}}$ in the projectile reference frame, with $\sigma^2 = \sigma_0^2 \frac{A_f(A_p - A_f)}{A_p - 1}$, and P, A_p, A_f being the fragment momentum in this frame, projectile mass number, and fragment mass, respectively. The value of Fermi momentum related parameter $\sigma_0 = 100$ MeV/c was chosen in agreement with the results of [11, 22]. The total ${}^4\text{He}$ fragmentation cross-sections into ${}^3\text{He}$, ${}^3\text{H}$, and D used in the program, were borrowed from measurements on Carbon target [32], and corrected for their $A^{1/3}$ dependence.

B) - In the coalescence model, the invariant differential production cross sections for composite fragments with mass A , are related to the nucleon production cross section by a simple power law:

$$(E_A \frac{d^3 N_A}{d\vec{p}_A^3}) = B_A \cdot (E_p \frac{d^3 N_p}{d\vec{p}_p^3})^A,$$

with $\vec{p}_A = A \cdot \vec{p}_p$. This relation provides straightforwardly the momentum spectrum of mass A fragments as a function of the nucleon spectrum at the same production angle. The inputs of the event cross section calculation then consist only of the value of the B_A parameter and of the proton production differential cross-section. The coalescence parameters for p induced collisions have been found to have approximately constant values through the energy range from 0.2 GeV/n up to 70 GeV/n [33]. The following values, averaged from [14, 17, 21, 29, 34], were used in the program: $B_2 = 2.5 \cdot 10^{-2}$ for deuteron, $B_3 = 2.5 \cdot 10^{-4}$ for ${}^3\text{He}$, $B'_3 = 4 \cdot 10^{-4}$ for ${}^3\text{H}$, and $B_4 = 4 \cdot 10^{-6}$ for ${}^4\text{He}$, in units $(\text{GeV}^2/c^3)^{(A-1)}$. The accuracy on these values is estimated to be within $\pm 30\%$ for B_2 , and $\pm 50\%$ for B_3 and B'_3 . See [17] for B_4 . The proton induced proton production was generated as described in [35] using the parametrization from [36], while for incident ${}^4\text{He}$ particles, the same spectral shape as for protons was used, with the appropriate scaling to take into account the experimental total reaction cross section [31] and proton production cross section (multiplicity) for ${}^4\text{He}$ collisions on nuclei [26, 37].

The simulation has been run for $2 \cdot 10^8$ incident primary proton and helium particles generated at the injection sphere. This number corresponds to a sampling time of $4 \cdot 10^{-12}$ s of the cosmic ray flux. The results are shown on figures 1 to 4. Note that no adjustable parameter was involved in the calculations.

The general features of the simulated sample are quite similar to those already reported in I for protons. In particular, concerning the trapping of particles in the earth magnetic field, the same trend

is observed for the population to be confined with a long lifetime (> 10 s) in the region of equatorial latitudes. The same class of low energy very long lifetime but low crossing multiplicity, quasi-polar population as observed in I, is found here, likely corresponding to the population of more outer belts than studied here.

Figure 1 shows the some basic distributions of the produced ${}^3\text{He}$ and D particles, crossing the detection altitude (no angular acceptance involved at this level). The fractional energy of the produced fragment with respect to the energy of the incident article (top left) shows a clear distinction between the coalescence yield at low energy and the approximately velocity-conserving fragmentation products at high energy. Also seen is the strong dominance of the D coalescence yield, larger than the ${}^3\text{He}$ yield by two orders of magnitude, and the much less different fragmentation yields, due to the particular structure of ${}^4\text{He}$ which fragments into D with a naturally higher multiplicity than in the general case. The rank distribution in the atmospheric cascade for ${}^3\text{He}$ (top right, solid histogram) displays a prominent peak for rank one. This originates from the fragmentation ${}^3\text{He}$ component which occurs mostly at the first interaction of the primary CR ${}^4\text{He}$. Coalescence particles are seen to be produced up to more than 8 generations of collision in the cascade. The mean production altitude (bottom left) predicted for deuterons (40 km) in agreement with our previous calculations (see [38] for the experimental context) is significantly lower than for (coalescence plus fragmentation) ${}^3\text{He}$ (51 km). This is also due to the fragmentation process which occurs at the first collision and thus at higher altitude on the average (dotted histogram). The ${}^3\text{He}$ coalescence yield (not shown) has a similar distribution as for D s. The same strong East-West effect (bottom right) responsible for the lepton asymmetry reported in [6], is also seen here as it could be expected.

Figure 2 shows the comparison between the flux spectra measured by AMS (full circle) [7] and the simulation results (histograms), taking into account the spectrometer acceptance (30 deg), for 3 bins in latitude. The solid histograms correspond to the ${}^4\text{He}$ CR flux above GC. It is seen that they reproduce fairly well the experimental distributions, with however a tendency to underestimate the experimental CR flux close to GC. This defect was not observed in our previous works on the protons [5] and lepton [6] flux. The dotted histograms correspond to ${}^3\text{He}$ particles produced by ${}^4\text{He}$ fragmentation. The expected yield is seen to be significant only above GC, and the differential flux appears to be more than two order of magnitude smaller than the primary ${}^4\text{He}$ flux, except for the few bins very close to the cutoff. This value is small compared to the known ${}^3\text{He}$ CR flux [39, 40, 41] which ratio to the CR ${}^4\text{He}$ flux is about 10% for this momentum range, i.e. about ten times larger than the value calculated here. This result is compatible with the AMS measurements (see figure 4 in [7]). The dashed and gray-shaded histograms correspond to CR p plus ${}^4\text{He}$ induced coalescence ${}^3\text{He}$ and ${}^4\text{He}$ flux respectively. As expected from the introductory discussion, the ${}^3\text{He}$ flux is more than one order of magnitude larger than for ${}^4\text{He}$. These flux are lying below GC, and the simulated ${}^3\text{He}$ spectra account pretty well for the measured spectra in magnitude and shape, with some underestimate of the data however in the higher subGC momentum range for the equatorial and intermediate latitudes.

Upper figure 3 shows the (downwards) ${}^3\text{He}$ particle spectrum measured by AMS, in kinetic energy per nucleon, integrated over the corrected geomagnetic (CGM, see I for the precise definition) latitude latitude range $|\theta_M| < 0.6$ rad, compared to the simulation results (coalescence yield, solid histogram). The calculated values are seen to be in agreement with the data within a factor of about 2 over the whole energy domain and over a dynamical range covering two orders of magnitude, which can be considered as a very good overall agreement. The small ${}^4\text{He}$ coalescence yield (dashed histogram) predicted is expected to be more than one order of magnitude smaller, a value compatible with the AMS conclusions in which an experimental upper limit of 10% for this ratio was set. Lower figure 3 compares the experimental (full circles) and simulated (histograms) energy-integrated ${}^3\text{He}$ flux below GC as a function of the geomagnetic latitude. The full histogram corresponds to the total expected yield. It accounts quite well for the measured flux except for the highest latitude bin. The dashed

histogram gives the ${}^4\text{He}$ induced contribution, which is seen to amount to 40-50% of the total yield. This is due to the combination of a larger total reaction cross section and larger proton multiplicity (with then a larger coalescence probability) with ${}^4\text{He}$ than with proton incident particles, which enhances the ${}^4\text{He}$ induced coalescence yield.

Figure 4 shows the expected spectral yields for ${}^2\text{H}$ and ${}^3\text{H}$ particles, for a set of bins in latitude. Note that although the two contributions were included, these yields are almost exclusively due to coalescence. The results for the ${}^2\text{H}$ spectra below GC are in very good agreement in magnitude and in shape with the preliminary AMS results [8]. This ability of the calculations to successfully and consistently reproducing both the ${}^3\text{He}$ and D flux at the same altitude of measurement with the same production model constitutes a very strong indication that these particles do originate from the same coalescence mechanism.

Some ${}^3\text{He}$ flux measurements have been reported recently at lower energies and larger distance from earth in the region of the inner belt [42]. This flux could not be definitely interpreted in the quoted work. It could certainly be investigated in the present approach.

In conclusion, it has been shown that the AMS measurements of the ${}^3\text{He}$ and D particle flux can be reproduced consistently and simultaneously, together with the proton secondary flux as reported in I, by a simulation incorporating the interactions between Cosmic Ray flux, earth magnetosphere and atmosphere, and assuming the ${}^3\text{He}$ and D particles to be produced by coalescence of nucleons in the CR proton and ${}^4\text{He}$ induced nuclear collisions with atmospheric nuclei. The ${}^4\text{He}$ fragmentation products appear not to contribute at a detectable level to the flux measured below the geomagnetic cutoff.

These results also clearly point to the interest for the future satellite experiments to have a particle identification capability covering this mass region and extending over a large kinetic energy range down to about 0.2 GeV per nucleon, in order to allow the experiments to collect data samples larger by more than two orders of magnitudes than those analyzed here, and then to make possible the achievement of a much more detailed investigation of the issues addressed in the present work.

References

- [1] C. Störmer, The Polar Aurora, Clarendon Press (Cambridge), 1955; S.F. Singer and A.M. Lenchek, Prog. in Elem. Part. and Cosm. Ray Phys. Vol 6, p 245, NHPC, 1962; E.C. Ray, J. Geophys. Res., 65(1960)1125; R. Konig, J. Geophys. Res. 86(1981)515
- [2] J. Alcaraz et al., Phys. Lett. B472(2000)215;
- [3] J. Alcaraz et al., Phys. Lett. B484(2000)10
- [4] J. Alcaraz et al., Phys. Lett. B490(2000)27
- [5] L. Derome et al., Phys. Lett. B 489(2000)1
- [6] L. Derome et al., astro-ph/0103474
- [7] J. Alcaraz et al., Phys. Lett. B494(2000)19
- [8] G. Lamanna, thesis, University of Perugia, 2000; G. Lamanna, AMS internal note 2000-07-02, july 2000; J. Alcaraz et al., the AMS collaboration, to be published
- [9] R.N. Bekmirzaev et al., Phys. At. Nucl. 58(1995)1548
- [10] M. Buénerd et al., Phys. Rev. Lett. 37(1976)1191; C.K. Gelbke et al., Phys. Rep. 42(1978)311

- [11] A.S. Goldhaber, Phys. Lett. B 53(1974)306
- [12] G. Westfall et al., Phys. Rev. Lett. 37(1976)1202
- [13] J. Gosset et al., Phys. Rev. C16(1977)629
- [14] G. Montarou et al., Phys. Rev. C44(1991)365
- [15] S. Das Gupta and A.Z. Mekjian, Phys. Rep. 72(1981)131
- [16] D.H. Boal, Phys. Rev. C25(1982)3068
- [17] S. Nagamiya et al., Phys. Rev. C24(1981)971
- [18] S.T. Butler and C.A. Pearson, Phys. Rev. 129(1963)836; A. Shwarzshild and C. Zupančič Phys. Rev. 129(1963)854
- [19] W.J. Llope et al., Phys. Rev. C52(1995)2004
- [20] V.B. Gavrilov et al., Sov. J. of Nucl. Phys. 41(1985)540
- [21] V.V. Abramov et al., Sov. J. of Nucl. Phys. 45(1987)845
- [22] J. Mougey et al., Phys. Lett. B 105(1981)25
- [23] A.S. Goldhaber and H.H. Heckman, Ann. Rev. Nucl. Sci. 28(1978)161
- [24] G. Bizard et al., Nucl. Phys. A 285(1977)461
- [25] L. Anderson et al., Phys. Rev. C 28(1983)1224
- [26] D. Armutliiski et al., Sov. J. of Nucl. Phys. 45(1987)649
- [27] P. Lipari, astro-ph/0101559, Jan 31, 2001.
- [28] S.V. Boyanirov et al., Sov. J. of Nucl. Phys. 47(1988)600
- [29] G.A. Safronov et al., Sov. J. of Nucl. Phys. 47(1988)966
- [30] J.R. Letaw, R.Silberberg, and C.H. Tsao, Ap.J. Suppl, 51(1983)271
- [31] J. Jaros et al., Phys. Rev. C18(1978)2273
- [32] A.Kh. Abdurakhimov et al., Nucl. Phys. A362(1981)376
- [33] J. Simon-Gillo et al., Nucl. Phys. A590(1995)477c
- [34] N. Saito et al., Phys. Rev. C49(1994)3211
- [35] L. Derome and M. Bunerd, Nucl. Phys. A688(2001)66
- [36] A.N. Kalinovski, M.V. Mokhov, and Yu.P. Nikitin, *Passage of high energy particles through matter*, AIP ed., 1989
- [37] S. Baskovic et al., Phys. At. Nucl. 56(1993)540
- [38] Particle Data Group, Eur. Phys. J. C15(2000)150

- [39] O. Reimer et al., ApJ., 496(1998)490
- [40] J.J. Beatty et al., ApJ. 413(1993)268
- [41] W.R. Webber et al., ApJ., 380(1991)230
- [42] J.P. Wefel et al., Proc. of 24th ICRC, Roma, Aug 28-sept 8, 1995, p1021.

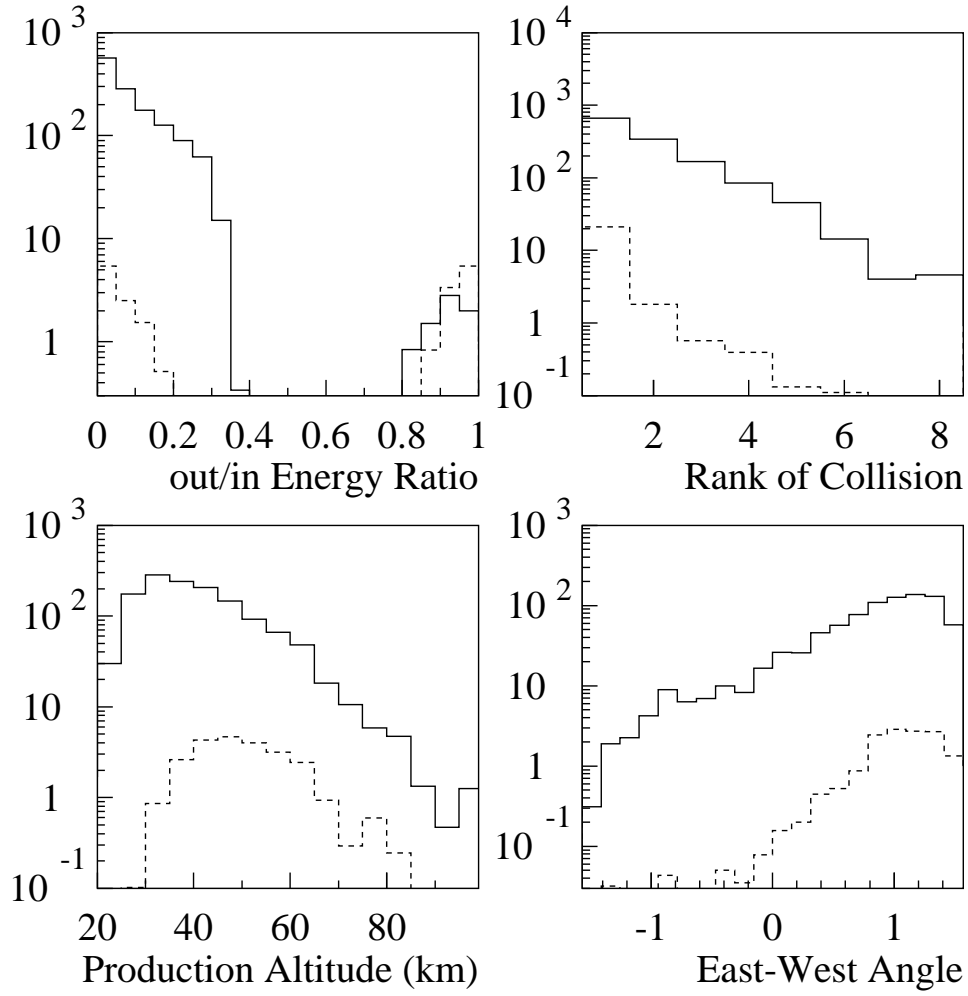


Figure 1: Features of the simulated samples for ${}^3\text{He}$ (dashed histograms) and D particles (solid histograms). From top to bottom and from left to right: Altitude of production (km), rank in the atmospheric cascade, fractional energy of particles, and East-West angle distributions (rad).

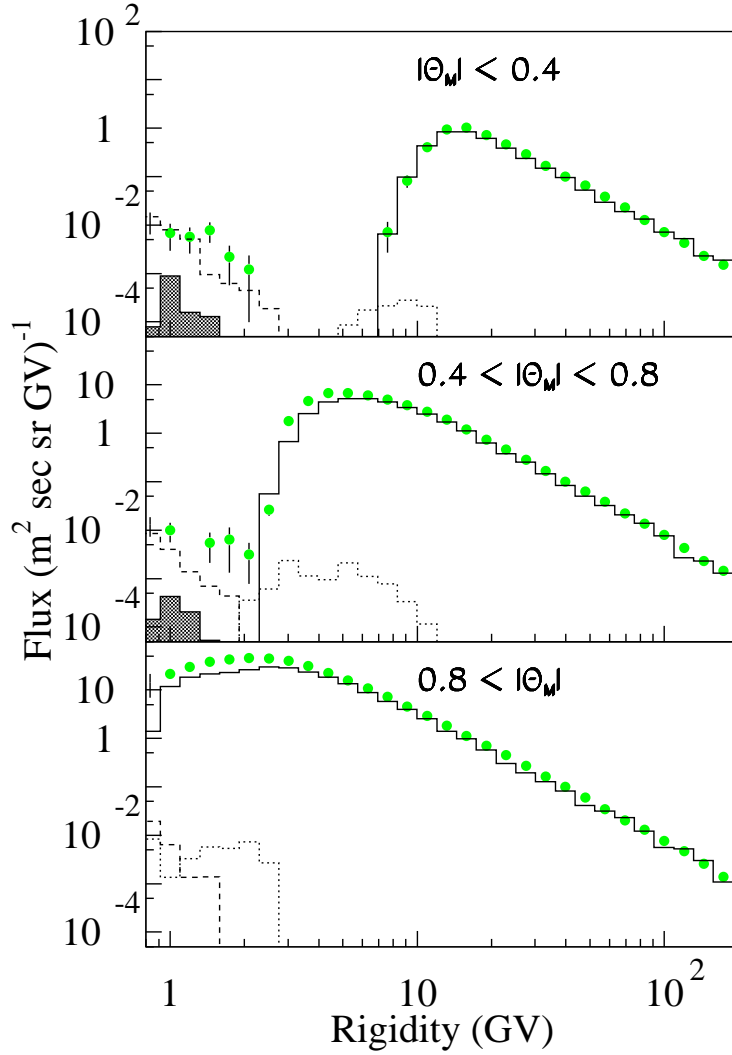


Figure 2: Comparison of the Helium spectra measured by AMS ([7] full circles) at various CGM latitudes θ_M , with the simulation results (histograms). Full line : ${}^4\text{He}$ above GC; Dotted: ${}^3\text{He}$ from ${}^4\text{He}$ fragmentation; Dashed: coalescence ${}^3\text{He}$; shaded: coalescence ${}^4\text{He}$. See text for details.

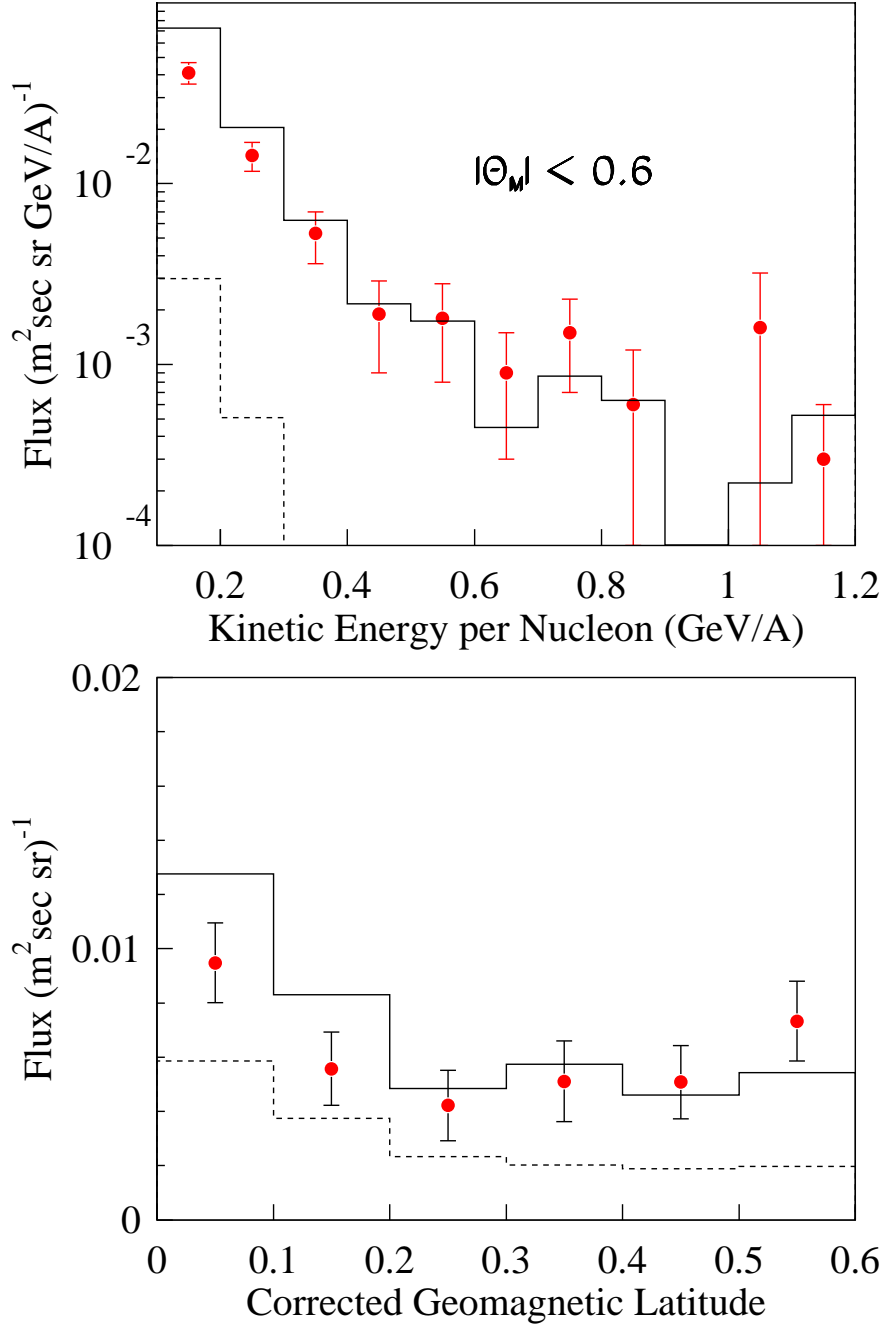


Figure 3: Top: Experimental energy spectrum of the subGC ${}^3\text{He}$ flux integrated over $\theta_M < 0.6$ rad, measured by AMS [7], compared to simulation results (solid histogram). The dashed histogram corresponds to the coalescence ${}^4\text{He}$ flux. Bottom: Energy-integrated ${}^3\text{He}$ experimental distribution ($E < 1.2$ GeV/A) as a function of the CGM latitude (full circles) compared to simulation results for proton and ${}^4\text{He}$ induced flux. The dashed histogram shows the ${}^4\text{He}$ induced contribution.

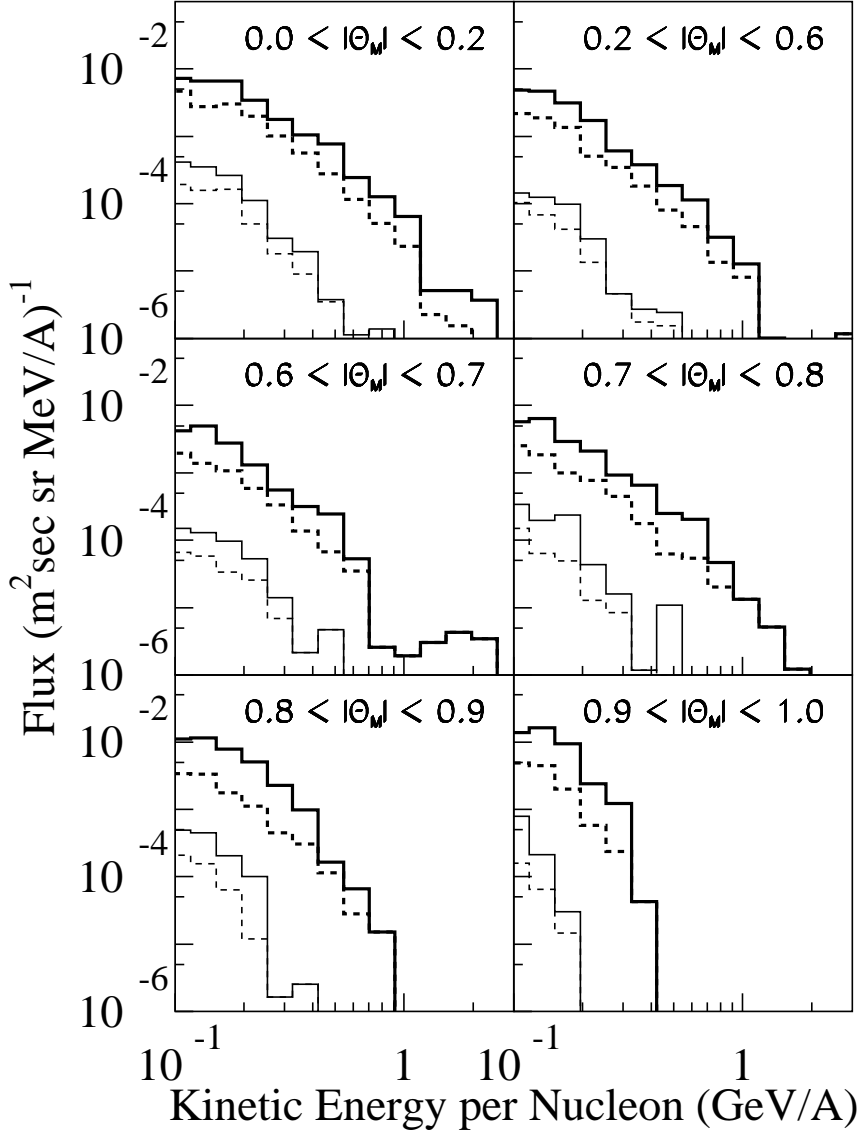


Figure 4: Prediction for the subGC flux of deuterium ${}^2\text{H}$ (thick histograms) and tritium ${}^3\text{H}$ particles (thin histograms) for various bins of latitude between equator and polar region (CGM bin values θ_M given in radian). Solid line : full (p plus ${}^4\text{He}$) yield; Dashed line : ${}^4\text{He}$ yield.